Surface Raman Spectroscopy of Chemistry at the Tris(8-hydroxyquinoline) aluminum/Ca Interface†

Robert J. Davis and Jeanne E. Pemberton*

Department of Chemistry, University of Arizona, 1306 E. University Boulevard, Tucson, Arizona 85721

Received: December 15, 2008

Surface Raman spectroscopy in ultrahigh vacuum is used to interrogate interfaces formed between tris(8-hydroxyquinoline) aluminum (Alq_3) and vapor-deposited Ca. Vapor deposition of Ca onto Alq_3 films results in the appearance of new vibrational modes consistent with the formation of a Ca−Alq_3 adduct in which Ca is bound through the O of Alq_3. In addition, the graphitic carbon is observed to form with the deposition of Ca onto Alq_3 films. The frequency and relative peak height ratios of graphitic D-band and G-band observed are consistent with more disordered sp^3-type carbon forming upon partial decomposition of the organic film.

Introduction

Tris-8-hydroxyquinoline aluminum (Alq_3) has become a common electroluminescent and electron transport material in organic light emitting diodes (OLEDs) due to its superb stability and luminescence properties.[1,2] Due to its prevalence and importance in device function, the interface of Alq_3 with cathodic metals has been examined extensively by UPS/XPS,[3−10] vibrational spectroscopy,[11−15] and theory[16−20] in an effort to relate interfacial chemical and electronic properties to device performance. Metals used as cathodes are commonly selected to have a low work function in order to minimize any barrier to electron injection from the cathode to the electron transport layer. Precise tuning of this charge injection barrier is essential to producing high efficiency devices. If the charge transfer rate between the metallic cathode and the organic transport layer is too low, overall device efficiency will be reduced, while if the charge transfer rate is significantly higher than the electron transport rate of the bulk organic layer, electrons will accumulate at the metal−organic interface also leading to a reduction in device performance. Thus, a precise understanding of the chemical and electronic interfacial properties is essential to designing high efficiency devices.

Ca has been effectively used as a cathode in high efficiency polymer-based devices based on PPV,[21] MEH-PPV,[22] and poly(9,9-dioctylfluorene)[23] while Ca is less commonly used in conjunction with Alq_3 in devices. Ca, with a work function of 2.8 eV,[3,10] would appear to be an ideal cathode material for use in conjunction with Alq_3 whose LUMO level has been placed by optical measurements at 2.9 eV,[24] leading to a minimal theoretical barrier to charge injection. A study of efficiency for devices incorporating Alq_3 with several low work function metals as cathodes, however, has reported that Ca/Alq_3 does not perform as well as might be expected.[25] The highest electroluminescent efficiency for interfaces using Alq_3 was observed by Stossel et al.[25] for Mg, having a work function of 3.7 eV, with a 10−15% dropoff in relative efficiency noted for lower work function metals, such as Ca (2.8 eV) and Li (2.95 eV). This trend in device performance is often attributed to other interfacial properties that can also affect charge transfer efficiency including the formation of new species through chemical reaction, interface dipole formation, and diffusion of materials at the interface. On the basis of the electron affinity of Alq_3, 2.9 eV,[26] and the ionization potentials of Al, Ca, and Mg of 6.0, 6.1, and 7.6 eV, respectively,[27] it is expected that an electron will be transferred from the metal atom to Alq_3 at the interface of these materials.

Theoretical studies of the interaction of Al with Alq_3 have reported stable metal−Alq_3 adducts in which the metal atom is bound to Alq_3 through the O atom of the 8-hydroxyquinoline (8-HQ) ligand, while studies of Mg with Alq_3 have reported Mg to be bound to both the O and C atoms of the 8-HQ ligand.[16−20] Shifts in the XPS core levels for the N 1s and O 1s core levels reported in studies of Mg−Alq_3 and Al−Alq_3 interfaces support the formation of such complexes.[5−10] Previous studies of these interfaces by Raman spectroscopy in this laboratory have reported the formation of new ν(M−O) modes and shifts in the ν(C−O), ν(C−N), and ν_{ring} modes of pristine Alq_3 upon deposition of Mg and Al onto Alq_3 thin films.[14,15] These spectral changes are also consistent with formation of metal−organic complexes in which Mg and Al are bound to Alq_3 through the O atom of 8-HQ.

DFT calculations of the interaction of Ca atoms with Alq_3 by Curioni and Andreoni have also found stable Ca−Alq_3 structures in which Ca is bound to one O atom of 8-HQ in *mer*-Alq_3 and to three O atoms in *fac*-Alq_3.[16] Interestingly, the binding energies for the calculated Ca−Alq_3 complexes (11 kcal/mol for Ca−*mer*-Alq_3, 23 kcal/mol for Ca−*fac*-Alq_3) are substantially lower than those reported for the Al−Alq_3 complexes (37 kcal/mol for Al−*mer*-Alq_3, 51 kcal/mol for Al−*fac*-Alq_3), indicating weaker binding for the Ca−Alq_3 system.[16] UPS and XPS studies of Ca−Alq_3 have reported that deposition of Ca onto Alq_3 films leads to the decomposition of the organic in a staged reaction, attributed to the formation of the Alq_3 radical anion at Ca coverages ≤4 Å and decomposition of Alq_3 at higher coverages as evidenced by peak splitting of the N and O 1s core levels and changes in elemental stoichiemometry.[3,4] Interestingly, partial decomposition of Alq_3 to graphitic carbon has been reported for Al−Alq_3 and Mg−Alq_3 in the Raman spectroscopy of these systems.[14,15] Vibrational modes associated with formation of amorphous, nanocrystalline graphitic carbon are present for these systems and attributed to a reaction of excess deposited metal with the metal−Alq_3

† Part of the "George C. Schatz Festschrift".

* To whom correspondence should be addressed. E-mail: pembertn@u.arizona.edu. Phone: 520-621-8245. Fax: 520-621-8248.

10.1021/jp8110698 CCC: $40.75
Published on Web 02/25/2009

complexes.[14,15] A similar decomposition reaction could explain the shift of the C 1s to lower binding energy reported in XPS studies of Ca−Alq_3.[3,4]

The high reactivity of these metal−organic interfaces further complicates efforts to characterize them. The potential for oxide formation by low work function metals such as Ca has been shown to degrade device performance and requires the use of ultrahigh vacuum (UHV) to prevent extrinsic interface reactions due to metal oxide formation.[28,29] Previous studies of the interaction of Al−*trans*-stilbene, Ag−Alq_3, Al−Alq_3, and Mg−Alq_3 by Raman spectroscopy in UHV have demonstrated the technique's high specificity and sensitivity to changes in structure and bonding at metal−organic interfaces.[14,15,30] In this study, Raman spectroscopy is used to assess the reactivity of Ca deposited onto Alq_3 thin films as a function of metal coverage in UHV.

Experimental Section

Ultrahigh Vacuum Chamber. Organic and metallic thin films were prepared and characterized in a custom-built ultrahigh vacuum (UHV) chamber.[14,15,30] Thin films were deposited in a sample preparation chamber separated by a 6 in. gate valve and analysis chamber. A 300 L s^{-1} turbomolecular pump, an ion pump, and two titanium sublimation pumps maintain a base pressure of 2×10^{-10} torr in the analysis chamber; working pressures were seldom above 10^{-9} torr. The ion and titanium sublimation pumps are liquid nitrogen-cooled to remove condensable gases (primarily H_2O).

Chemically polished Ag substrates were mounted on a 1.5 m Advanced Research Systems DE-204B closed-cycle He-cooled cryogenic translatable arm that could be cooled to a base operating temperature of 30 K. This arm can be translated between the sample preparation and analysis chambers at temperature. Temperature was controlled in these studies using a Cryo-Con Model 34 cryogenic temperature controller using a type K, Chromel-AuFe thermocouple at the bottom of the coldfinger within close proximity of the stub.

Materials. 8-Hydroxyquinoline, aluminum salt (99.995%), was obtained from Aldrich and was degassed at 250 °C at 10^{-9} torr for 6 h prior to deposition. Calcium crystalline dendritic pieces (99.98%) were obtained from Alpha Aesar and degassed at 400 K at $\sim 1 \times 10^{-9}$ torr for 1 h prior to remove any metal oxide. A 1.25 cm diameter Ag (111) disk (99.999%, Alfa Aesar) was used as the underlying substrate for all experiments.

Procedures. The procedure for obtaining chemically polished Ag surfaces has been outlined previously.[31,32] Alq_3 films were prepared on Ag substrates held at 300 K, similar to the conditions used in the fabrication of OLED devices, and are spectroscopically consistent with the formation of amorphous or α-Alq_3.[33−35] Ca was deposited after degassing onto the Alq_3−Ag sample held at ∼60 K from Al_2O_3-coated W/Ta crucibles to ensure a sticking coefficient of 1 for the deposited metals and to prevent the desorption of any volatile reaction products. Film deposition was monitored differentially using a multifilm deposition monitor (Maxtek TM-400) and a gold-coated quartz sensor crystal (Maxtek SC-101). The sensor was held at room temperature for Alq_3 deposition but cooled with liquid N_2 during metal deposition; reported values of coverage represent mass thicknesses of the metal assuming bulk density.

Raman spectra were acquired by moving the sample stub into the glass cell at the end of the analysis chamber. Radiation of 514.5 nm with 20 mW power at the sample was provided by a Coherent Innova 350C Ar^+ laser. Light was incident on the sample at 60°, and scattered photons were collected at 30° with respect to the surface normal. Collected radiation was collimated and focused onto the front entrance slit of a single monochromator (Spex 270M) with a 1200 gr/mm grating and set for a 5 cm^{-1} spectral bandpass. A holographic SuperNotch Plus filter (Kaiser Optical Systems) was used to reduce Rayleigh scattering. A 1340 × 400 pixel, thinned, back-illuminated CCD (Roper Scientific model 400-EB) held at −95 °C was used for detection. Typical integration times varied from 10 to 30 min per acquisition. Spectra were calibrated using Ar^+ emission lines. Peak fitting of Raman spectra was accomplished with Grams/32 using 100% Gaussian peaks. Peaks at frequencies associated with intense Alq_3 modes were fit using peak frequencies (±5 cm^{-1}) and relative intensities (±10%) determined by Halls and Aroca[33] with full-width-at-half-maximum (fwhm) values of 15 cm^{-1} (±10 cm^{-1}). Modes associated with graphitic carbon were fit using five broad bands using peak frequencies (±10 cm^{-1}), relative intensities (±50%), and fwhm (±50%) described by Ferrari and Robertson.[36] All additional spectral features were fit with broad bands that were allowed to vary in frequency by ±10 cm^{-1}, in fwhm by ±10 cm^{-1}, and intensity by ±50%.

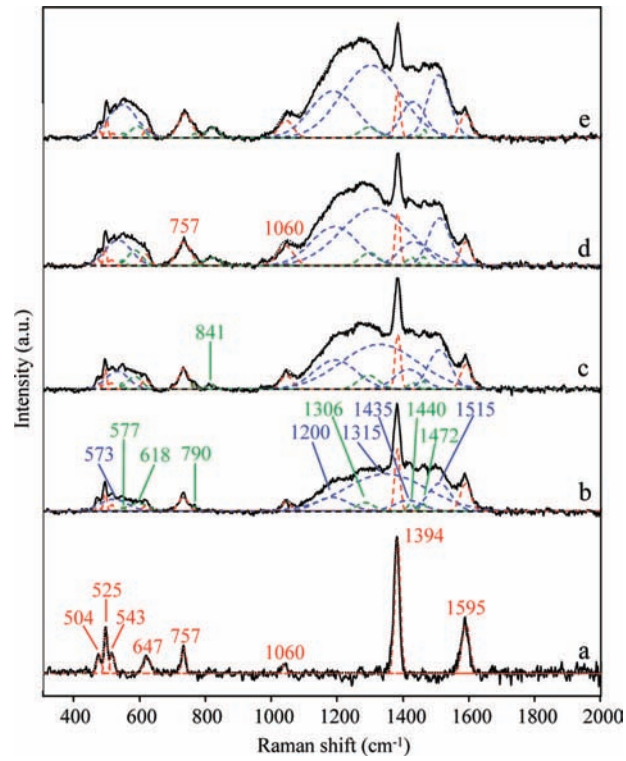

Figure 1. Peak fitting of Raman spectra of 150 Å Alq_3 films after Ca deposition of (a) 0, (b) 5, (c) 10, (d) 15, and (e) 20 Å mass thickness. Raw Raman spectrum (black solid lines), overall fit envelope (black dashed lines), Alq_3 modes (red dashed lines), Ca−Alq_3 reaction product modes (green dashed lines), and graphitic carbon modes (blue dashed lines).

Results and Discussion

Ca has a low atomic ionization potential that supports electron transfer to the conjugated 8-HQ ring of Alq_3, and UPS/XPS measurements have demonstrated a strong Ca interaction with the organic layer.[3,4] Figure 1 shows Raman spectra at 90 K of a pristine 150 Å Alq_3 film on Ag before and after deposition of Ca layers ranging in mass thickness from 5 to 20 Å. With the deposition of 5 Å Ca in Figure 1b, the Alq_3 modes at 1595, 1394, 543, 525, and 504 cm^{-1} exhibit a 30−40% intensity decrease compared to those from the pristine Alq_3 thin film. Broad modes also appear for 5 Å Ca on Alq_3 from 1100 to

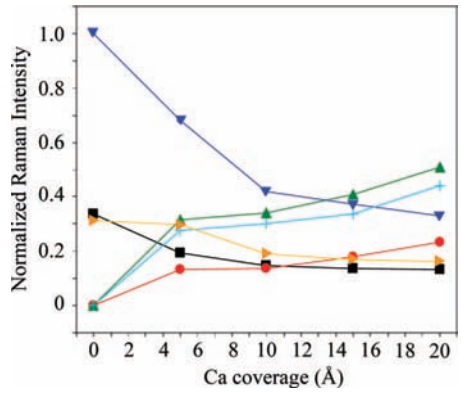

Figure 2. Normalized Raman peak intensity as function of metal coverage for Ca deposited onto Alq_3 for [ring deformation + ν(Al−O)] at 525 cm^{-1} (black square), graphitic carbon δ_{ring} at 573 cm^{-1} (red circle), graphitic carbon D-band at 1315 cm^{-1} (green up triangle), [ν_{ring} + δ(C−H)] at 1394 cm^{-1} (blue down triangle), graphitic carbon G-band at 1515 cm^{-1} (light blue cross), and ν_{ring} at 1595 cm^{-1} (yellow right triangle). All modes normalized to intensities of respective bands in pristine Alq_3.

1600 cm^{-1} in the region associated with the formation of graphitic carbon.

In order to more readily observe the differing spectral contribution from Alq_3, graphitic carbon, and any other reactive products, peak fitting was employed. Peak fitting of the region from 1100 to 1600 cm^{-1} using 100% Gaussian bands reveals two intense, broad bands at 1505 and 1265 cm^{-1} whose breadth and frequency are consistent with the presence of graphitic carbon.[36] In addition, a broad mode present at 577 cm^{-1} corresponds to a weak out-of-plane vibrational mode of amorphous graphite, previously only reported in sp^3-rich graphite.[37] The peak at 1515 cm^{-1} is attributed to the G-band of graphitic carbon, with the known low-frequency asymmetry of the G-band fit using an additional Gaussian band at 1435 cm^{-1}. The peak at 1315 cm^{-1} is attributed to the D-band of graphitic carbon. As with the G-band, the known low-frequency asymmetry of the D-band is fit using an additional broad band at 1200 cm^{-1}. Similar modes have been previously observed in Raman spectra for the Mg−Alq_3 and Al−Alq_3 systems and are attributed to a decomposition reaction resulting from the interaction of excess metal atoms with metal−Alq_3 complexes formed at the interface. Interestingly, the intensity ratio of the D-band to G-band is higher than that reported for Mg−Alq_3 (∼0.7) or Al−Alq_3 (∼0.5),[14,15] indicating that the graphitic carbon formed at the Ca−Alq_3 interface is more disordered than for the other metal−Alq_3 systems. The ratio of peak intensities of the fit bands for the D-band to the G-band is ∼1.1, indicating the presence of largely amorphous carbon with some sp^3 character.[36] The amount of graphitic carbon also increases monotonically from 5 to 20 Å Ca in Figure 2 while the ratio of the D:G band remains relatively constant. The lack of a D′-band at 1605−1620 cm^{-1} was observed in both the Mg−Alq_3 and Al−Alq_3 systems and indicates small grain graphitic carbon with little clustering of graphite into larger sheets.[36] The low frequency asymmetry of both the D-band and G-band graphitic modes, as shown in the fit peaks at 1200 and 1435 cm^{-1}, respectively, is also more pronounced for Ca−Alq_3 than that reported for other metal−Alq_3 systems. A similar increase is the low frequency asymmetry of the D- and G-bands of graphitic carbon has been noted after sputtering of highly ordered polycrystalline graphite (HOPG) with N^+ ions.[38] The authors of this study attributed the increased asymmetry of the D- and G-bands to ion implantation into the graphite film, leading to more discontinuities in the crystalline structure. A similar argument may explain the highly disordered graphitic carbon observed in the Ca−Alq_3 films in which excess Ca, as well as other decomposition products of Alq_3, hinder the formation of graphite with long-range order.

Upon deposition of 5 Å of Ca onto Alq_3, new modes also appear at 1472, 1440, 1306, 790, 618, and 577 cm^{-1} that are not consistent with modes for Alq_3, although these modes appear in frequency regions consistent with structures closely related to 8-hydroxyquinoline and/or with Alq_3 modes that are not normally Raman-active.[14,33] The new modes present at 1472, 1440, and 1306 cm^{-1} with Ca coverage of 5 Å are in the frequency region are associated with Alq_3 ring stretching and ring deformation modes. The decrease in frequency of these modes relative to those for pristine Alq_3 at 1595 and 1394 cm^{-1} is explained by binding of Ca to Alq_3, resulting a lowering of ring electron density, leading to a decrease in the force constant. The product mode at 1306 cm^{-1} is additionally assigned to a ν(C−O) mode shifted from the mode at 1335 cm^{-1} for pristine Alq_3.[14,33] A similar shift in the ν(C−O) mode has been reported for both Al-Alq_3 and Mg-Alq_3,[14,15] respectively, and is attributed to binding of the metal.

The absence of any observable ν(Ca−C) modes from 300 to 500 cm^{-1} in Figure 1b suggests that Ca does not bond directly to the ring. Thus, it can be concluded that the shifts in ring breathing modes must be an indirect electronic effect due to removal of ring electron density by interaction of Alq_3 with the deposited Ca. New modes also appear at 790 cm^{-1} with 5 Å Ca deposited and at 841 cm^{-1} at 10 Å Ca deposited in the region associated with $\delta(C-H)_{wag}$ and δ_{ring} modes, respectively. These modes are shifted to lower frequency from the $\delta(C-H)_{wag}$ at 862 cm^{-1} and δ_{ring} at 804 cm^{-1},[33] again as a consequence of a reduction in electron density in the π-system of Alq_3 upon binding of Ca.

The mode at 618 cm^{-1} in Figure 1b is assigned as a ν(Ca−O) resulting from binding of Ca to the O atom of the 8-HQ in Alq_3. Binding of the inserted Ca in this position is congruous with the theoretical structures determined by Curioni and Andreoni[16] in which the lowest energy structure has the inserted Ca bound through the O atom of a *mer*-Alq_3 molecule as depicted in Figure 3. The authors additionally found a structure for the Ca−(*fac*-Alq_3) adduct in which the Ca was proposed to bind to three O atoms; this structure is more stable than the Ca−(*mer*-Alq_3) structure with 1-coordinate binding to O. These authors also theorized that *mer*-Alq_3, the more stable Alq_3 isomer that is presumed to be dominant in thin films, may convert to *fac*-Alq_3 upon interaction with deposited Al.[16] However, the multitude of spectral changes in the spectral region of the Raman spectrum associated with Al−N and Al−O bonding upon Ca deposition prohibits definitive confirmation of the conversion from *mer*- to *fac*-Alq_3, and either Ca−(*fac*-Alq_3) or Ca−(*mer*-Alq_3) or both are possible products. It should be noted that the binding energies calculated for Ca−(*fac*-Alq_3) and Ca−(*mer*-Alq_3) complexes of 23 and 11 kcal/mol, respectively, are significantly lower than those calculated for the Al−(*fac*-Alq_3) and Al−(*mer*-Alq_3) complexes of 51 and 39.5 kcal/mol, respectively.[16] These values indicate that the Ca−Alq_3 complex is less stable than the Al−Alq_3 adduct and may explain the strong tendency toward decomposition to graphitic carbon noted for this system.

Choong et al.,[4] in their UPS study of this interface, observed for the deposition of 0.5 Å Ca onto Alq_3 the formation of a gap state along with a concomitant loss of Alq_3 spectral features. The gap state indicates a significant change in chemical and

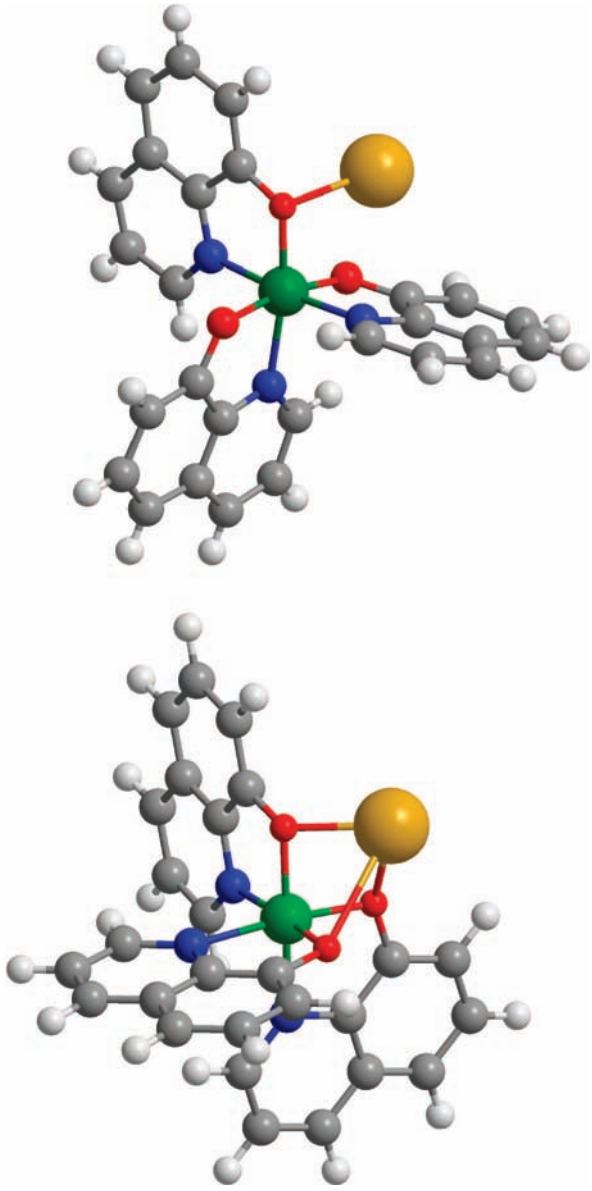

Figure 3. Proposed Ca−Alq_3 adduct structures in which Ca is bonded to Alq_3 through ligand O atoms for *mer*-isomer (top) of Alq_3 and *fac*-isomer (bottom) of Alq_3. C, H, N, O, and Al atoms of Alq_3 shown in gray, white, blue, red, and green, respectively; vapor-deposited Ca atom shown in yellow.

electronic properties, even at low Ca coverages, as would be expected for the formation of a Ca−Alq_3 adduct. XPS measurements by the same authors demonstrated a shift in the C, N, O 1s core levels to higher binding energies by ∼1 eV, that was attributed to band bending resulting from a change in the interface dipole with 4 Å Ca deposited onto Alq_3 films. At higher coverages of Ca (15−30 Å), an additional weak intensity N 1s core level peak is reported at ∼0.5 eV lower binding energy from the N 1s of the Alq_3 film.[4] A significantly more intense O 1s core level peak is observed at higher Ca coverages, with a shift by 1 eV to lower binding energy compared the O 1s of Alq_3. The presence of this new band supports an increase in electron density upon the proposed binding of Ca with the O atom of 8-HQ and is confirmed by the shift in ν(C−O) to lower frequency and the appearance a new ν(Ca−O) in Figure 1b−e.

Broadening of the ν_{ring} at 757 cm^{-1} also occurs for 5−20 Å Ca deposited. A similar broadening has been reported for this mode in the Raman spectra of Al−Alq_3 and Mg−Alq_3.[14,15] The

TABLE 1: Raman Peak Frequencies and Assignments for a Pristine Alq_3 Film and after Deposition of 20 Å of Ca

peak frequency (cm^{-1})			
literature Alq_3[a]	150 Å Alq_3	20 Å Ca on Alq_3	mode assignment[b]
1595	1595	1595	ν_{ring}
		1515	graphite G-band
		1472	ν_{ring}
1471		1440	ν_{ring}
		1435	graphite G-band
1424	1424		$\nu_{ring} + \delta$(C−H)
1394	1394	1394	$\nu_{ring} + \delta$(C−H)
1386			δ(C−H) + ν_{ring}
		1315	graphite D-band
1335		1306	$\nu_{ring} + \nu$(C−O) + δ(C−H)
		1200	graphite D-band
1060	1060	1060	ν(C−O) + δ(C−H)
862		841	$\delta(C-H)_{wag}$
804		790	δ_{ring}
757	757	757	ν_{ring}
647	647	647	ν(Al−O) + ν(Al−N) + δ_{ring}
		618	ν(Ca−O)
577		577	$\delta_{ring} + \delta$(Al−O−C)
		573	graphite δ_{ring}
541	543	543	ν(Al−O) + ν(Al−N) + δ_{ring}
525	525	525	$\delta_{ring} + \nu$(Al−O)
504	504	504	δ_{ring}
470	470		CH torsion

[a] From ref 23. [b] Assignments for Alq_3 from ref 23 and those for graphite from refs 24 and 28.

lack of changes to the ν(Al−O), ν(Al−N), and δ(Al−O−C) modes upon exposure to Ca that were reported for Mg−Alq_3[15] and Al−Alq_3[14] may be due to a weaker interaction between Ca and Alq_3 than the interaction reported for Mg and Al. This weak interaction results in the magnitudes of shifts in Alq_3 electron density upon bonding with the metal that are not as significant in Ca/Alq_3.

The spectral changes that are observed for the Ca−Alq_3 system are summarized in Table 1. These changes suggest that a complex interface is formed that is composed of highly disordered graphitic carbon as well as a Ca−Alq_3 adduct that has a structure similar to that proposed in Figure 3, in which the deposited Ca is bound through the O atom of the 8-HQ ligand. It is also important to note that the intensities of the Ca−Alq_3 product modes relative to those of pristine Alq_3 are lower than that reported for either Al−Alq_3 or Mg−Alq_3.[14,15] The smaller degree of Ca−Alq_3 adduct formation may result from the instability of the Ca−Alq_3 complex or from an inability of Ca to penetrate into the Alq_3 film. The atomic radius of Ca (1.80 Å) is considerable larger than that of either Mg or Al (1.50 and 1.25 Å).[27] Figure 4 shows a Chem 3D rendition of a Ca inserted between two molecules in α-Alq_3. The large size of the Ca atom places it in close contact with the neighboring Alq_3 ligand, separated by only 1.5−2.0 Å, and may limit penetration of Ca into the Alq_3 film, thereby retarding the formation of the Ca−Alq_3 complex.

The temperature used for the deposition of Ca metal films in this study of 60 K was chosen to ensure a high sticking coefficient of Ca on the Alq_3 film and retention of any volatile reactive species. This temperature is less than that typically used in the construction of organic electronic devices from these materials. Although this temperature is not believed to significantly alter the structures of the Alq_3 film or products formed between Ca and Alq_3, cooling of the samples may result in reduced diffusion of the deposited metal, limiting the depth of

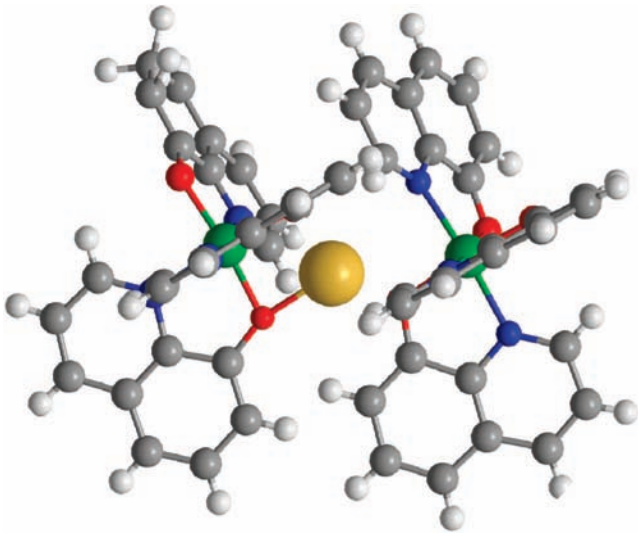

Figure 4. Proposed structure for Ca inserted into α-crystal phase of *mer*-Alq_3. C, N, O, and Al atoms of Alq_3 shown in gray, blue, red, and green, respectively; vapor-deposited Ca atom shown in yellow.

the reaction with Alq_3 and creating a narrower metal−organic interfacial region than may be formed in real devices produced at room temperature.

Conclusions

Raman spectra for Alq_3 films exhibit significant spectral changes after deposition of 5−20 Å Ca. The loss in intensity of all major Alq_3 modes coupled with the appearance of new modes supports the partial reactive conversion of Alq_3 to a new product in which Ca is bound to Alq_3 through the O atom of 8-HQ as evidenced by the appearance of a new ν(Ca−O) mode at 618 cm^{-1}. The shifts in ν_{ring} and ν(C−O) further support interaction of the deposited Ca with an O atom of Alq_3 and a subsequent shift in electron density in the π-system of the ligand. The relative intensities of the Ca−Alq_3 product modes observed here are significantly lower than those reported previously for both the Al−Alq_3 and Mg−Alq_3 products, indicating, as proposed by Curioni and Andreoni, that the Ca−Alq_3 complex may be significantly less stable than the other metal−Alq_3 complexes.[16]

The appearance and growth of graphitic carbon modes at 1515, 1435, 1315, 1200, and 573 cm^{-1} indicate degradation of Alq_3 to graphitic carbon after the deposition of Ca. The frequencies and relative intensity ratio of the D-band and G-band modes of graphitic carbon indicate that highly disordered graphite with a large sp^3 character is formed as a result of partial decomposition of the organic film.[36] This graphitic carbon is considerably more disordered and contains more sp^3 character than the graphitic carbon previously reported for both Mg−Alq_3 and Al−Alq_3, illustrating that important chemical differences are present at the reactive interfaces of these seemingly similar metals with Alq_3.

The presence of even a small amount of graphitic carbon at the Ca−Alq_3 interface has profound implications for interfacial electronic structure and conductivity in functioning electronic devices. The graphitization reaction reported in this study at 90 K is expected to be retained at room temperature, commensurate with the conditions used for device fabrication, although diffusion may limit the extent of the reaction and breadth of the interfacial region at 90 K. The formation of a Ca−Alq_3 complex at the interface may also have several effects on charge injection. The Ca−Alq_3 complex likely lies at an energy level between the bulk Alq_3 film and the metal Fermi level, as observed by the formation of a gap state in UPS examination of the interface.[5] Such an interfacial state may act as an intermediate hopping state between the metal and Alq_3, thus lowering the thermal energy required for injection.[39] The presence of Ca−Alq_3 complexes as well as decomposition products also likely creates disorder within the Alq_3 film at the interface, further broadening the interfacial region and the energy distribution of interfacial states. This broadening may also lower the effective thermal energy required for electron injection.

Lastly, the presence of decomposition products at the Ca/Alq_3 interface may further broaden the energy distribution of the interfacial states toward lower energies. Notably, the graphitic carbon formed at Ca/Alq_3 has a higher sp^3 character than that observed at either Al/Alq_3 or Mg/Alq_3. This more disordered carbon contains a higher degree of defect sites which may serve as traps for injected electrons, lowering the efficiency of charge transfer across the interface. Conversely, the presence of additional lower energy states from the disordered graphitic carbon may aid in electron injection by serving as hopping sites between the metal and Alq_3 levels. The electroluminescent efficiencies reported by Stossel et al.[25] for the Ca/Alq_3 interface suggest that the former behavior may dominate in these systems, or in other words, the high number of defect sites in the graphitic carbon trap injected electrons. Despite similar electron affinities for Mg and Ca, Raman spectra of these metal−organic interfaces clearly show that the structures of both the metal−Alq_3 adducts and the graphitic carbon formed in these systems are substantially different.

Acknowledgment. The authors gratefully acknowledge support of this research by the National Science Foundation.

References and Notes

(1) Tang, C. W.; Vanslyke, S. A. *Appl. Phys. Lett.* **1987**, *51*, 913.
(2) Tang, C. W.; Van Slyke, S. A.; Chen, C. H. *J. Appl. Phys.* **1989**, *65*, 3616.
(3) Park, Y.; Choong, V. E.; Hsiesh, B. R.; Tang, C. W.; Wehrmeister, T.; Mullen, K.; Gao, Y. *J. Vac. Sci. Technol., A* **1997**, *15*, 2574.
(4) Choong, V. E.; Mason, M. G.; Tang, C. W.; Gao, Y. *Appl. Phys. Lett.* **1998**, *72*, 2689.
(5) Rajagopal, A.; Kahn, A. *J. Appl. Phys.* **1998**, *84*, 355.
(6) Le, Q. T.; Yan, L.; Choong, V.-E.; Forsythe, E. W.; Mason, M. G.; Tang, C. W.; Gao, Y. *Synth. Met.* **1999**, *102*, 1014.
(7) Le, Q. T.; Yan, L.; Gao, Y.; Mason, M. G.; Giesen, D. J.; Tang, C. W. *J. Appl. Phys.* **2000**, *87*, 375.
(8) Shen, C.; Hill, I. G.; Kahn, A.; Schwartz, J. *J. Am. Chem. Soc.* **2000**, *122*, 5391.
(9) Shen, C.; Kahn, A.; Schwartz, J. *J. Appl. Phy.* **2001**, *89*, 449.
(10) Yan, L.; Mason, M. G.; Tang, C. W.; Gao, Y. L. *Appl. Surf. Sci.* **2001**, *175*, 412.
(11) Sakurai, Y.; Salvan, G.; Hosoi, Y.; Ishii, H.; Ouchi, Y.; Seki, K.; Kampen, T. U.; Zahn, D. R. T. *Appl. Surf. Sci.* **2002**, *190*, 382.
(12) Sakurai, Y.; Hosoi, Y.; Ishii, H.; Ouchi, Y.; Salvan, G.; Kobitski, A.; Kampen, T. U.; Zahn, D. R. T.; Seki, K. *J. Appl. Phys.* **2004**, *96*, 5534.
(13) Sakurai, Y.; Yokoyama, T.; Hosoi, Y.; Ishii, H.; Ouchi, Y.; Salvan, G.; Kobitski, A.; Kampen, T. U.; Zahn, D. R. T.; Seki, K. *Synth. Met.* **2005**, *154*, 161.
(14) Davis, R. J.; Pemberton, J. E. *J. Phys. Chem. C* **2008**, *112*, 4364.
(15) Davis, R. J.; Pemberton, J. E. *J. Am. Chem. Soc.*, submitted.
(16) Curioni, A.; Andreoni, W. *J. Am. Chem. Soc.* **1999**, *121*, 8216.
(17) Zhang, R. Q.; Lu, W. C.; Lee, C. S.; Hung, L. S.; Lee, S. T. *J. Chem. Phys.* **2002**, *116*, 8827.
(18) Meloni, S.; Palma, A.; Schwartz, J.; Kahn, A.; Car, R. *J. Am. Chem. Soc.* **2003**, *125*, 7808.
(19) Meloni, S.; Palma, A.; Kahn, A.; Schwartz, J.; Car, R. *J. Appl. Phys.* **2005**, *98*, 23707.
(20) Takeuchi, K.; Yanagisawa, S.; Morikawa, Y. *Sci. Technol. Adv. Mater.* **2007**, *8*, 191.
(21) Blom, P. W. M.; deJong, M. J. M.; Vleggaar, J. J. M. *Appl. Phys. Lett.* **1996**, *68*, 3308.
(22) Parker, I. D. *J. Appl. Phys.* **1994**, *75*, 1656.

(23) Brown, T. M.; Friend, R. H.; Millard, I. S.; Lacey, D. J.; Burroughes, J. H.; Cacialli, F. *Appl. Phys. Lett.* **2001**, *79*, 174.
(24) Burrows, P. W.; Forrest, S. R. *Appl. Phys. Lett.* **1994**, *64*, 2285.
(25) Stossel, M.; Staudigel, J.; Steuber, F.; Simmerer, J.; Winnacker, A. *Appl. Phys. A: Mater. Sci. Process.* **1999**, *68*, 387.
(26) Schlaf, R.; Parkinson, B. A.; Lee, P. A.; Nebesny, K. W.; Armstrong, N. R. *Appl. Phys. Lett.* **1998**, *73*, 1026.
(27) *CRC Handbook of Chemistry and Physics,* 64th ed.; Weast, R. C., Ed.; CRC Press: Boca Raton, FL, 1984.
(28) Shen, C. F.; Hill, I. G.; Kahn, A. *Adv. Mater.* **1999**, *11*, 1523.
(29) Broms, P.; Birgerson, J.; Salaneck, W. R. *Synth. Met.* **1997**, *88*, 255.
(30) Hawkridge, A. M.; Pemberton, J. E. *J. Am. Chem. Soc.* **2003**, *125*, 624.
(31) Smolinski, S.; Zelenay, P.; Sobkowski, J. *J. Electroanal. Chem.* **1998**, *442*, 41.
(32) Tiani, D. J.; Pemberton, J. E. *Langmuir* **2003**, *19*, 6422.
(33) Halls, M. D.; Aroca, R. *Can. J. Chem.* **1998**, *76*, 1730.
(34) Brinkmann, M.; Gadret, G.; Muccini, M.; Taliani, C.; Masciocchi, N.; Sironi, A. *J. Am. Chem. Soc.* **2000**, *122*, 5147.
(35) Curry, R. J.; Gillin, W. P.; Clarkson, J.; Batchelder, D. N. *J. Appl. Phys.* **2002**, *92*, 1902.
(36) Ferrari, A. C.; Robertson, J. *Phys. Rev. B* **2000**, *61*, 14095.
(37) Tamor, M. A.; Vassell, W. C. *J. Appl. Phys.* **1994**, *76*, 3823.
(38) Watanabe, H.; Takahashi, K.; Iwaki, M. *Nucl. Instrum. Methods Phys. Res., Sect. B* **2007**, *257*, 549.
(39) Baldo, M. A.; Forrest, S. R. *Phys. Rev. B* **2001**, *64*, 85201.

JP8110698